Effects of snow cover on soil freezing, water movement, and snowmelt infiltration: A paired plot experiment

Yukiyoshi Iwata,[1] Masaki Hayashi,[2] Shinji Suzuki,[3] Tomoyoshi Hirota,[4] and Shuichi Hasegawa[5]

Received 6 April 2009; revised 14 April 2010; accepted 29 April 2010; published 2 September 2010.

[1] A dramatic reduction in soil frost depth has been reported for Hokkaido Island of northern Japan over the last 20 years. Since soil frost strongly affects snowmelt infiltration and runoff, the reduction in frost depth may have altered the water and nutrient cycles in this region. A paired-plot experiment was conducted in an agricultural field in Tokachi, Hokkaido, to compare the movement of soil water at different frost depths, controlled by manipulating the depth of snow cover. Snow was removed to enhance soil freezing in the treatment plot and was undisturbed in the control plot. The soil froze to a maximum depth of 0.43 m under the treatment plot and 0.11 m under the control plot. During the freezing period, the amount of upward soil water flux toward the freezing front in the treatment plot was more than double that in the control plot. During the snowmelt period, infiltration of meltwater was unimpeded by the thin frozen layer in the control plot, whereas the relatively thick frozen layer in the treatment plot impeded infiltration and generated 63 mm of runoff. These results clearly show that the changes in the timing and thickness of snow cover deposition can cause a dramatic reduction of frost depth and change in the soil water dynamics.

Citation: Iwata, Y., M. Hayashi, S. Suzuki, T. Hirota, and S. Hasegawa (2010), Effects of snow cover on soil freezing, water movement, and snowmelt infiltration: A paired plot experiment, *Water Resour. Res.*, *46*, W09504, doi:10.1029/2009WR008070.

1. Introduction

[2] Many cold regions in the world experience an annual top down freezing of the soil during the winter months. However, recent studies have demonstrated an association between climate warming and a reduction in soil-frost penetration depth [*Frauenfeld et al.*, 2004; *Hirota et al.*, 2006] and the frozen period [*Cutforth et al.*, 2004] in cold regions around the world. A frozen soil layer generally increases the amount of snowmelt runoff by decreasing soil permeability and thereby impeding infiltration [*Bayard et al.*, 2005]. This results in increased soil erosion [*Øygarden*, 2003], reduced soil moisture recharge [*Gray et al.*, 2001] and deep percolation [*Johnsson and Lundin*, 1991], and an increased magnitude of spring freshet [*Shanley and Chalmers*, 1999; *Unoki et al.*, 2003]. As the depth and duration of soil frost decreases in cold regions, snowmelt infiltration is expected to increase, which may affect the aforementioned processes. The development of soil frost results in a very low soil matric potential at the freezing front, which induces a large potential gradient [*Miller*, 1980]. This results in the movement of water from the deeper soil to the freezing front, which significantly influences frost heaving [*Hohmann*, 1997] and nutrient transport [*Gray and Granger*, 1986].

[3] Despite the potential importance of changes in frost depth, few studies have quantitatively examined the relationship between frost depth and the dynamics of soil water. Recent advances in monitoring methods, such as time domain reflectometry (TDR), have allowed for the automatic monitoring of water content in frozen soils [e.g., *Stähli et al.*, 1999; *Nyberg et al.*, 2001; *Flerchinger et al.*, 2006]. However, comprehensive field measurements of soil water movement in frozen soils are rare due to the logistical and technical difficulty of conducting fieldwork in cold environments. As a result, it is difficult to examine long-term changes in soil water movement associated with climate change. Data from a region that presently has thick soil frost may provide insight into the past conditions of regions that have undergone frost-depth reduction. However, infiltration in frozen soils is affected by soil permeability, water content, repeated thawing and refreezing, and many other factors and their complex interactions [*Stähli*, 2005]. Therefore, a quantitative comparison of soil-water dynamics for different frost depths requires data collected from similar soil and climatic conditions. Numerical models [e.g., *Stähli et al.*, 1996; *Gray et al.*, 2001] may provide a useful tool for sensitivity analysis, but such models need to be calibrated and validated using site-specific field data. Comparative field studies are impeded by the difficulty of finding sites with deep soil frost next to similar sites with shallow frost. Alternatively, artificial snow cover removal decreases the thermal insulation of soil surfaces and increase frost depths.

[1]National Agricultural Research Center for Hokkaido Region, NARO, Memuro, Japan.
[2]Department of Geoscience, University of Calgary, Calgary, Alberta, Canada.
[3]Department of Bioproduction and Environment Engineering, Tokyo University of Agriculture, Tokyo, Japan.
[4]National Agricultural Research Center for Hokkaido Region, Sapporo, Japan.
[5]Field Science Center for Northern Biosphere, Hokkaido University, Sapporo, Japan.

0043-1397/10/2009WR008070

This approach has been used in forest environments to obtain soil temperature and moisture data under considerably different snow and frost depth conditions [*Thorud and Duncan*, 1972; *Hardy et al.*, 2001; *Decker et al.*, 2003], and may be useful for studying the effects of snow and frost depth on soil-water dynamics in other environments.

[4] In the Tokachi District of northern Japan, annual maximum frost depth has decreased from > 0.4 m to 0.05–0.2 m over the past 20 years, while average winter (December–February) air temperature showed no systematic trend [*Hirota et al.*, 2006]. The penetration of soil frost is generally enhanced by low air temperature and reduced by the thermal insulation of snow cover. The effect of latter is determined by the thickness and the timing (early versus late) of snow cover [e.g., *Luetschg et al.*, 2008]. From the analysis of meteorological variables and frost depths, *Hirota et al.* [2006] showed that the decrease in frost depth in Tokachi is caused by the earlier development of snow cover in recent years, compared to previous years, which insulates the ground earlier and decreases the effective time window for soil-frost penetration. This shift in the timing of snow cover development is believed to be related to a shift in synoptic-scale meteorology associated with climate change [*Hirota et al.*, 2006]. *Iwata et al.* [2008a] found that a relatively thin (annual maximum < 0.2 m) frozen layer under present climatic conditions does not impede snowmelt infiltration, suggesting that a dramatic shift in winter soil-water dynamics and snowmelt infiltration/runoff may have occurred in this region, due to the recent decrease in frost depth. However, it is difficult to compare the present and past soil-water dynamics and snowmelt infiltration/runoff processes in Tokachi, due to the lack of detailed field data from the pre-shift period.

[5] The purpose of this study is to compare soil water dynamics and snowmelt infiltration under present soil-frost conditions with those under past conditions simulated by removing snow cover to increase the effective time window of soil freezing. The specific research objectives are (1) to quantify soil-water movement during a winter period in two adjacent plots under natural and simulated soil frost conditions, (2) to determine the factors controlling the differences in snowmelt infiltration, and (3) to gain insight into the influence of frost-depth reduction on the agricultural environment of Tokachi.

2. Materials and Methods

2.1. Study Site

[6] This study was conducted at an experimental field located in the town of Memuro in the central part of Tokachi District, Hokkaido, Japan (Figure 1a), and operated by the National Agricultural Research Center for Hokkaido Region (143°05′E/42°53′W). Between 1979 and 2006, mean annual precipitation was 957 mm and mean monthly air temperature was −8.7°C for January and 18.0°C for July at the Memuro meteorological station, located 2.5 km west of the study site (Japan Meteorological Agency, Source of the archived meteorological data, March 2009, http://www.data.jma.go.jp/obd/stats/etrn/index.php). The study site is covered by volcanic-ash soil, which has a low bulk density, high porosity, and high hydraulic conductivity (Table 1) [*Iwata et al.*, 2008a]. The soil is underlain by a gravel layer at a depth of 1.3 m, and the water table in this area occurs at a depth of 8 m [*Oka*, 2000]. Large desiccation cracks are absent from the soil profile, based on visual observation in soil pits. The site has very little topographic relief (less than 1% slope).

[7] Two 5 × 5 m plots were located adjacent to each other (Figure 1b). Snow cover was manipulated in one plot (treatment plot), whereas natural conditions were maintained in the other (control plot). Based on long-term data from the study site [*Hirota et al.*, 2006], the average annual maximum frost depth (±one standard deviation) was 0.13 m (±0.07 m) and the average annual maximum snow cover thickness was 0.85 m (±0.20 m) during 1997–2005. In contrast, the average annual maximum frost depth was 0.38 m (±0.14 m) and annual maximum snow cover thickness was 0.47 m (±0.19 m) during 1986–1996. Therefore, we aimed to achieve a maximum frost depth of 0.4 m and a snow cover thickness of 0.5 m in the treatment plot to simulate the 1986–1996 conditions. The study was conducted from November 2005 to April 2006. Snow cover was removed after each snowfall event, several times between December 19 and January 13. To avoid further frost penetration, snow was artificially replaced after frost depth reached 0.4 m. As a result, the amount of snow in the treatment plot was comparable to that in the control plot at the onset of snowmelt (see results in section 3). Prior to the site installation, oats were planted in the summer of 2005 and harvested in September. After harvest, the soil was plowed to a depth of 0.15 m and mixed with plant residues.

2.2. Site Instrumentation and Snow Measurement

[8] Soil water content was monitored using a TDR system (TDR100; Campbell Scientific inc.) with 0.3-m long, three-rod probes (CS605). The probes were installed horizontally into the exposed face of a soil pit at a depth interval of 0.1 m from 0.05 to 1.05 m (Figure 1c). The pit was backfilled after the installation. To calibrate the probes, soil samples were collected from individual soil horizons, air-dried, and repacked in cylindrical PVC containers (0.083 m in internal diameter and 0.34 m in length) to approximately the same bulk density as that of the respective soil horizon (Table 1). The probes were inserted into the samples and soil water content was adjusted to desired values by adding distilled water to the top of the sample. After adding the water, the top was covered with plastic sheet to prevent evaporation, and apparent soil dielectric permittivity was determined once the output of the TDR probes had stabilized (usually one day after adding water). Polynomial calibration functions were used to calculate water content from dielectric permittivity for individual soil horizons. The root-mean squared (RMS) error of calibration functions ranged between 0.004 and 0.012 $m^3\ m^{-3}$. The water content measured by TDR in frozen soil is generally considered to represent liquid water content, as the dielectric permittivity of ice is similar to that of solid soil particles [*Stein and Kane*, 1983; *Suzuki*, 2004].

[9] Soil matric-potential was measured continuously through the winter at depths of 0.9 and 1.0 m using specifically designed tensiometers equipped with an insulating material and a small heat source [*Iwata and Hirota*, 2005a, 2005b]. These tensiometers were installed in a separate soil pit located 2 m away from the TDR probes (Figure 1b).

[10] Soil temperature was monitored in the same soil pit as the TDR probes. Copper-constantan thermocouples were installed from the surface down to 1.0-m depth (Figure 1c).

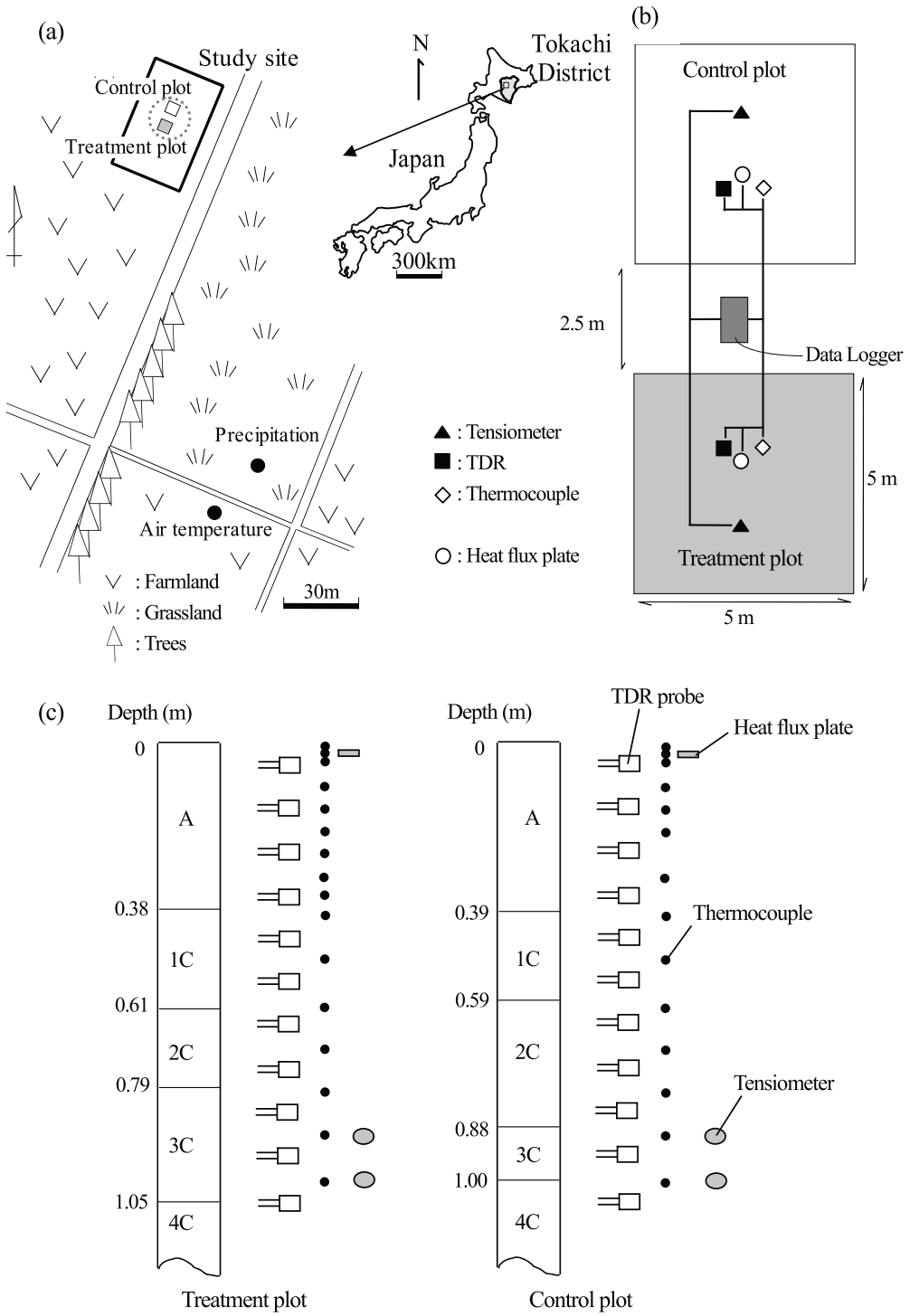

Figure 1. (a) Location of the study site, (b) layout of the instruments, and (c) soil profiles and depths of the sensors.

Soil was considered frozen when temperature was below 0°C [*Iwata et al.*, 2008b]. A heat-flux plate (REBS, HFT1.1) was installed at a depth of 0.02 m to monitor ground heat flux (Figure 1c). The flux plate was calibrated against independent flux estimates obtained during May–October 2006 using the combination method [*Hirota et al.*, 2001; *Sauer*, 2002], which combines the calorimetric method with an estimate of conductive flux at the bottom of soil profile. Volumetric heat capacity for the calorimetric calculation was estimated from specific heat, density, and volumetric fraction of individual phases [*Iwata et al.*, 2008a, equation 5]. Thermal conductivity of volcanic-ash soil is generally much lower than other types of mineral soils [*Kasubuchi*, 1975]. Therefore, the model of *Johansen* [1977], modified for

Table 1. Soil Profiles and Physical Characteristics of the Study Site[a]

Soil Horizon	A	1C	2C	3C	4C
Treatment plot depth (m)	0–0.38	0.38–0.61	0.61–0.79	0.79–1.05	1.05+
Control plot depth (m)	0–0.39	0.39–0.59	0.59–0.88	0.88–1.00	1.00+
Soil texture	L–CL	S_iL	CL	SCL	C
Dry bulk density (Mg m^{-3})	0.82	0.66	0.84	1.04	1.03
Porosity (m^3 m^{-3})	0.68	0.76	0.69	0.63	0.63
Saturated hydraulic conductivity (m s^{-1})	7.0×10^{-6}	4.0×10^{-5}	6.3×10^{-5}	2.3×10^{-4}	8.8×10^{-5}

[a]For soil texture, L is loam, CL is clay loam, S_iL is silt loam, SCL is sandy clay loam, and C is clay.

volcanic-ash soil by *Yamazaki et al.* [2003], was used to estimate thermal conductivity from dry bulk density, porosity, particle density, quartz content, and water content [*Iwata et al.*, 2008b].

[11] The soil pit data were recorded as 10-min average values by a Campbell Scientific CR-23X data logger. Precipitation and air temperature were continuously monitored at a meteorological station located 100 m from the study site (Figure 1a). Precipitation was measured using an overflow-type tipping-bucket rain gauge (Yokogawa Electric Corp., B071–20) with a heated water reservoir and a windshield (Yokogawa Electric Corp., RT-4). Air temperature was measured at 1.9 m above the ground using a resistive platinum sensor (Vaisala, HMP45A).

[12] Snow cover thickness and snow water equivalent (SWE) were measured manually twice a week at 0900h. SWE was measured at each plot using a 50-mm internal diameter aluminum snow-survey tube. Since evaporation rates from the snow surface during snowmelt are very small (<0.5 mm d^{-1}) compared to snowmelt rates at the study site [*Hayashi et al.*, 2005], daily snowmelt (M; mm d^{-1}) was calculated from the difference in SWE between two subsequent measurements plus the amount of precipitation that occurred between the measurements.

2.3. Calculation of Soil Water Storage and Flux

[13] Soil water storage was calculated for a soil profile extending from 0 to 1.1-m depth. The soil profile was divided into 11 layers, each 0.1 m thick. The TDR probes at depths of 0.05, 0.15, …, 1.05 m represented the layers of 0–0.1, 0.1–0.2, …, 1.0–1.1 m, respectively. Soil water flux (q_{95}) at 0.95-m depth was calculated from Darcy's law for unsaturated soil using the tensiometer data from 0.9 m and 1.0 m, with positive values indicating upward flux. Unsaturated hydraulic conductivity (k) at 0.95-m depth was calculated as a function of matric-potential head (ψ) using the arithmetic mean of the two tensiometer outputs. To define the conductivity function $k(\psi)$, the conductivity of soil samples was measured in the laboratory using the steady state method [*Hasegawa and Sakayori*, 2000] for -1.4 m $< \psi < 0.0$ m, and the one step method [*Doering*, 1965] for $\psi < -1.4$ m. Triplicate undisturbed soil cores, 0.113 m in diameter and 0.05 m in length, were collected from the 3C horizon (Table 1) corresponding to tensiometer depths. To take into consideration the hysteresis of $k(\psi)$, the steady state method was applied to wetting and drying processes.

[14] Soil water flux (q_z; mm d^{-1}) at a given depth (z) between the bottom of frozen layer and 1.1-m depth was calculated using the water balance equation:

$$q_z = q_{95} - \Delta S_{z-95}/\Delta t (z < 0.95 \text{ m}) \quad (1a)$$

$$= q_{95} + \Delta S_{z-95}/\Delta t (z > 0.95 \text{ m}) \quad (1b)$$

where ΔS_{z-95} is the change in the amount of liquid water stored (mm) in the soil layer between z and 0.95 m during a time interval (Δt; d).

[15] To quantify snowmelt infiltration through frozen soil, the top 0.95 m of the soil profile was divided into two layers, F and U (Figure 2). The boundary between the two layers is set at depths of 0.4 m in the treatment plot and 0.1 m in the control plot, which roughly coincide with the seasonal maximum frost depth in the two plots (see section 3.1). For both plots, almost all of the F layer was

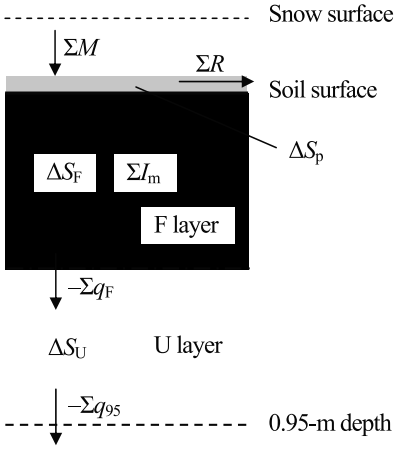

ΣM: snowmelt + rain
ΣR: runoff from the study plot
ΔS_p: change in surface storage
ΔS_F: change in liquid-water storage in F layer
ΣI_m: amount of soil ice melt
Σq_F: cumulative water flux at the bottom of F layer
ΔS_U: change in liquid-water storage in U layer
Σq_{95}: cumulative water flux at the bottom of U layer

Figure 2. Schematic diagram of soil water balance during the snowmelt period. The thickness of F layer is 0.4 m in the treatment plot and 0.1 m in the control plot.

frozen at the start of snowmelt on March 10 (frost depth was 0.39 m in the treatment plot and 0.11 m in the control plot). The liquid-phase water balance of the F layer is written as

$$\Sigma M + \Sigma I_m - \left(\Sigma R + \Delta S_p\right) = \Delta S_F - \Sigma q_F \quad (2)$$

were ΣM is the sum of snowmelt and liquid precipitation (mm) during a calculation period, ΣI_m is the amount of soil ice melt (mm), ΔS_F is the change in liquid-water storage (mm), Σq_F is the total soil water flux crossing the bottom of the F layer (mm), and $\Sigma R + \Delta S_p$ is the residual term, which is considered to be the sum of runoff and the change in surface storage or ponding (mm), respectively. The Σq_F was calculated by applying equation (1a) to the bottom of the F layer. Thus, the total q_F for a calculation period is given as

$$-\Sigma q_F = \Delta S_U - \Sigma q_{95} \quad (3)$$

where ΔS_U is the change in storage of liquid water in the U layer (Figure 2). Note that the bottom of the U layer is at 0.95-m depth and the sign of q_{95} is positive upward. It follows from equations (2) and (3) that

$$\Sigma R + \Delta S_p = \Sigma M - (\Delta S_F - \Sigma I_m + \Delta S_U - \Sigma q_{95}) \quad (4)$$

where $\Delta S_F - \Sigma I_m + \Delta S_U - \Sigma q_{95}$ represents snowmelt infiltration. The detailed calculation methods for determining individual terms in equation (4), as well as uncertainty estimates, are described in the auxiliary material.[1] A brief summary of calculation methods are presented below.

[16] The ΣI_m in equation (2) was calculated from the latent heat consumed by the melting of soil ice (ΔH_l; J m^{-2}) during a calculation period, using the energy balance equation for the F layer

$$\Delta H_l = \Sigma G_f - \Sigma G_s - \Delta H_f + \Sigma Q_a \quad (5)$$

where ΣG_f is the total heat flux at the bottom of the F layer (positive upward), ΣG_s is the total heat flux at the soil surface, ΔH_f is the change in sensible heat stored in the F layer, and ΣQ_a is the advective energy input by infiltrating water at the soil surface. The ΣI_m is equal to ΔH_l divided by the latent heat of fusion.

[17] The ΣG_f was calculated using the combination method (see section 2.2), and ΣG_s was approximated by the heat flux plate data. The calculation of ΔH_f requires an estimate of bulk soil volumetric heat capacity, which in turn requires an estimate of volumetric ice fraction (f_i) in the F layer. The initial value of f_i was estimated from the water balance calculation (see section 3.2). The value of f_i was updated at each calculation step by subtracting ΣI_m from the previous volume of ice. The ΣQ_a was calculated as a product of infiltration amount, volumetric heat capacity of water, and the temperature of infiltrating water, which was approximated by the soil surface temperature measured by the surface thermocouple. The magnitude of ΣQ_a was much smaller than other terms in equation (5) for most of the snowmelt period, as the soil surface temperature remained close to 0°C (see section 3).

3. Results

3.1. Overview

[18] Figure 3 shows daily mean values of air temperature, soil heat flux at 0.02-m depth (G_s), soil temperature, liquid water content, soil matric potential head, and the hydraulic gradient at 0.95-m depth. Daily precipitation, snow cover thickness, and snow water equivalent (SWE) are also shown in Figure 3. The soil started to freeze in late November, as indicated by the decrease in soil temperature (Figure 3f) and liquid water content (Figure 3g). The freezing is caused by the upward G_s (Figure 3e) induced by the low air temperature (Figure 3b). Soil freezing progressed similarly in both plots until December 19, when the first snow removal occurred in the treatment plot (Figure 3c). The rate of decrease in soil temperature slowed after December 19 in the control plot as the thick (>0.3 m) snow cover reduced the magnitude of G_s (Figures 3c and 3e). In contrast, G_s increased (Figure 3e) and soil temperature and liquid water content in the treatment plot continued to decrease steadily after December 19 under a very thin snow cover until January 13, when snow was put back on the treatment plot to prevent further penetration of the freezing front.

[19] The maximum frost penetration depth, which occurred in late February, was 0.11 m in the control plot and 0.43 m in the treatment plot (Figure 3f). Minimum soil temperature in the frozen layer was lower in the treatment plot (0 to −6°C) than in the control plot (0 to −2°C) (Figure 3f). Soil matric potential head at 0.9-m depth was much lower in the treatment plot (−5.8 m) than in the control plot (−2.7 m) (Figure 3h). The peak magnitude of hydraulic gradient at 0.95-m depth was 14 in the treatment plot and 1 in the control plot (Figure 3i), indicating a larger driving force for upward water movement toward the freezing front in the treatment plot.

[20] A 19 mm rainfall event occurred on February 26 (Figure 3a). The infiltration of rainwater increased soil water content in the shallow zone in both the treatment and control plot (Figure 3g). In the control plot, liquid water content below the frozen layer increased (Figure 3g) after the rain event, indicating the infiltration of snowmelt and rainwater through the frozen layer. A similar change in liquid water content did not occur in the treatment plot.

[21] Snowmelt started on March 10 (Figure 3d), and liquid water content at all depths increased rapidly in the control plot and remained nearly constant until the end of the snowmelt period (Figure 3g). In the treatment plot, liquid water content below 0.4-m depth increased only gradually during March (Figure 3g). Snow cover melted completely by March 22, but developed again after a new snowfall on March 29 (Figure 3c). The second phase of snowmelt started on April 6 and ended on April 17. The frozen layer persisted until the end of second snowmelt period in the treatment plot, but disappeared after the first melt phase in the control plot (Figures 3c and 3f).

[22] The maximum frost depth was 0.43 m and maximum snow cover thickness was 0.43 m in the treatment plot. These values are close to the target values of 0.4 m for frost depth and 0.5 m for snow cover, and reasonably simulated average soil frost and snow cover conditions of 1986–1996.

[1] Auxiliary materials are available in the HTML. doi:10.1029/2009WR008070.

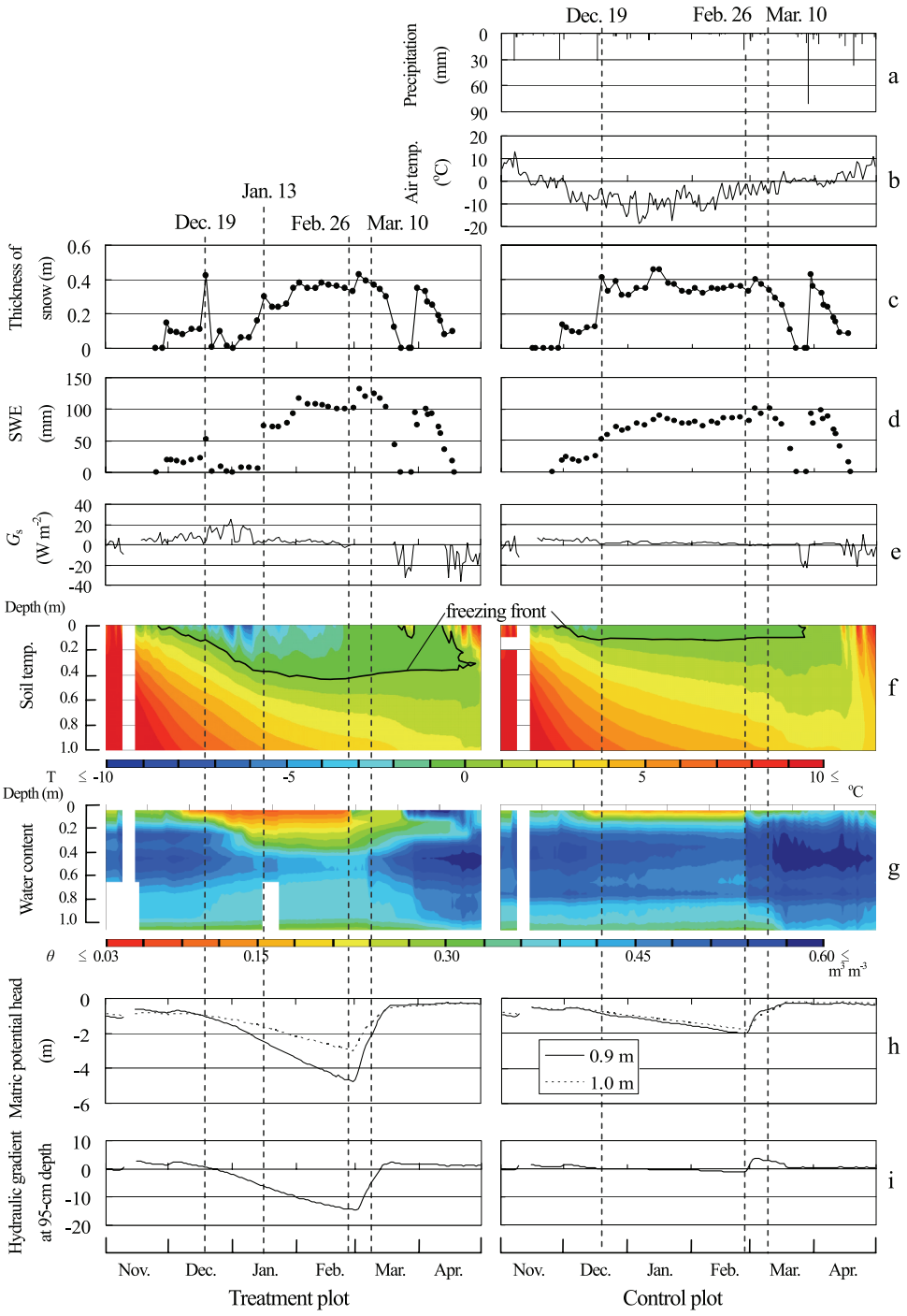

Figure 3. Time series of (a) precipitation, (b) air temperature, (c) thickness of snow cover, (d) snow water equivalent (SWE), (e) heat flux at the depth of 0.02 m (G_s), (f) soil temperature, (g) liquid soil water content, (h) matric potential head, and (i) hydraulic gradient from November 2005 to April 2006. The data gap in G_s, soil temperature, liquid soil water content, matric potential head, and hydraulic gradient is caused by instrumental problems.

[23] Physical processes during the observation period can be described in four stages: (1) top-down freezing accompanied by the upward soil water flow from the unfrozen soil to the freezing front under a thin snow cover, (2) no further advance of the freezing front under a thick snow cover, (3) rapid infiltration of rain and snowmelt water causing the temperature to increase in the frozen soil, and (4) snowmelt infiltration and soil thawing. In the following, we will present water flux calculations during the stages 1 and 4.

3.2. Upward Soil Water Flux Under the Frozen Layer

[24] Unsaturated hydraulic conductivity showed mild hysteresis for high (>−1 m) values of matric potential (Figure 4). Therefore, two separate $k(\psi)$ functions are used for −1.4 m <

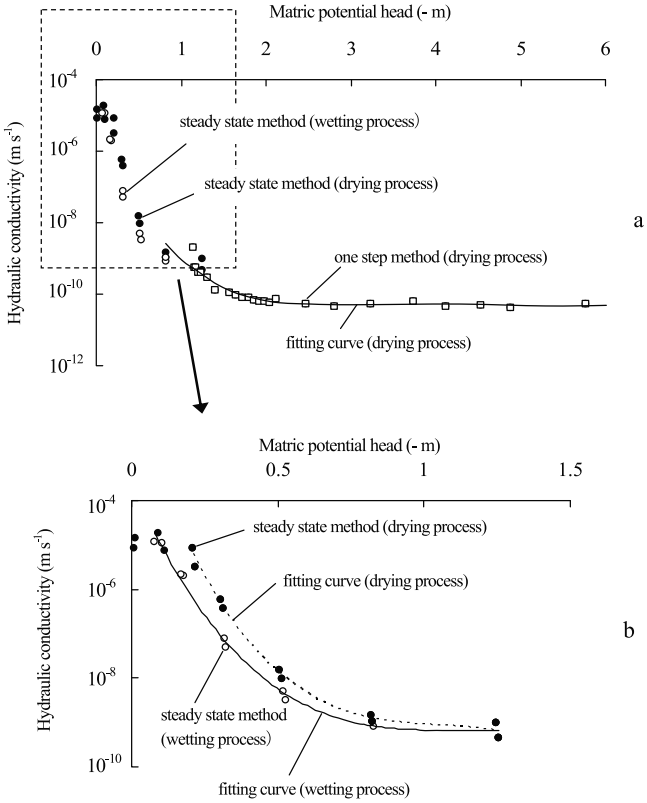

Figure 4. Relationships between soil hydraulic conductivity and matric potential head for soil samples collected from 3C horizon.

$\psi < 0.0$ m, and a single function was used for $\psi < -1.4$ m. The least squares regression was used to fit polynomial $k(\psi)$ functions to the measured data:

$$\begin{aligned}\log(k) &= 1.62 \times 10^{-4}|\psi|^6 - 7.50 \times 10^{-3}|\psi|^5 + 0.121|\psi|^4 \\ &\quad - 0.935|\psi|^3 + 3.74|\psi|^2 - 7.46|\psi| - 4.44(\psi < -1.4\text{ m}) \\ &= -5.80|\psi|^3 + 18.4|\psi|^2 - 19.8|\psi| \\ &\quad - 1.83(-1.4\text{m} < \psi < 0.0\text{ m, drying}) \\ &= -3.93|\psi|^3 + 13.3|\psi|^2 - 14.9|\psi| \\ &\quad - 3.63(-1.4\text{ m} < \psi < 0.0\text{ m, wetting}) \end{aligned} \quad (6)$$

where k is expressed in [m s^{-1}] and ψ in [m]. The RMS error of regression was 0.130 (unitless on logarithmic scale) for $\psi < -1.4$ m, 0.110 for -1.4 m $< \psi < 0.0$ m in drying process, and 0.126 for -1.4 m $< \psi < 0.0$ m in wetting process.

[25] Figure 5 shows the depth profile of average soil water flux below the freezing front (i.e., bottom of the frozen layer) over three 10-day periods before snowmelt for both study plots. Soil water flux below 0.2 m was negative (i.e., downward) for December 1–10 (Figure 5) in both plots due to the infiltration of rainwater in late November (Figure 3a). Flux was positive at all depths for January 1–10 (Figure 5) in both plots as water moved toward the freezing front, driven by the negative hydraulic gradient (Figure 3i). Noting that this is the period with a thick snow cover in the control plot and a very thin snow cover in the treatment plot (Figure 3c), the large difference in the magnitude of fluxes between the two plots demonstrates the effect of snow removal. The difference was relatively small for February 1–10 (Figure 5) after snow cover was put back on the treatment plot.

[26] Cumulative soil water flux crossing the depth of 0.4 m in the treatment plot was 20 mm during the snow removal period (December 20 to January 13). In contrast, cumulative flux at 0.4-m depth was 4 mm in the control plot, indicating a strong effect of snow cover in the control plot. During the period of similar snow cover conditions between the two plots (January 14 – February 25), the cumulative fluxes were 13 and 10 mm in the treatment and control plots, respectively, suggesting a relatively small difference between the two plots.

[27] Before the freezing started on November 27, the F layer (0–0.4 m) in the treatment plot had 165 mm of water. The total flux entering the bottom of the F layer in this plot was 39 mm between November 27 and February 25. The liquid water content in the F layer did not increase during this period (Figure 3g), indicating that the added water froze in the F layer. Therefore, the total amount of water (liquid + ice) in the F layer on February 25 was estimated to be 204 mm (= 165 + 39). The TDR data for the treatment plot indicate that the F layer had 87 mm of liquid water on February 25, meaning that the amount of ice in the F layer was 117 mm (= 204 – 87) on February 25. Similar water balance calculations for the control plot showed that the amount of ice in the F layer (0–0.1 m) was 47 mm on February 25.

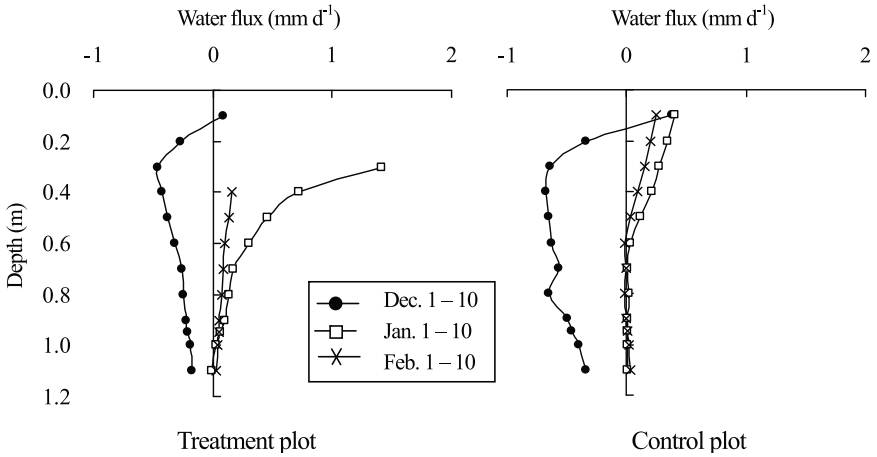

Figure 5. Average soil water flux below the frozen layer over three 10-day periods during soil freezing.

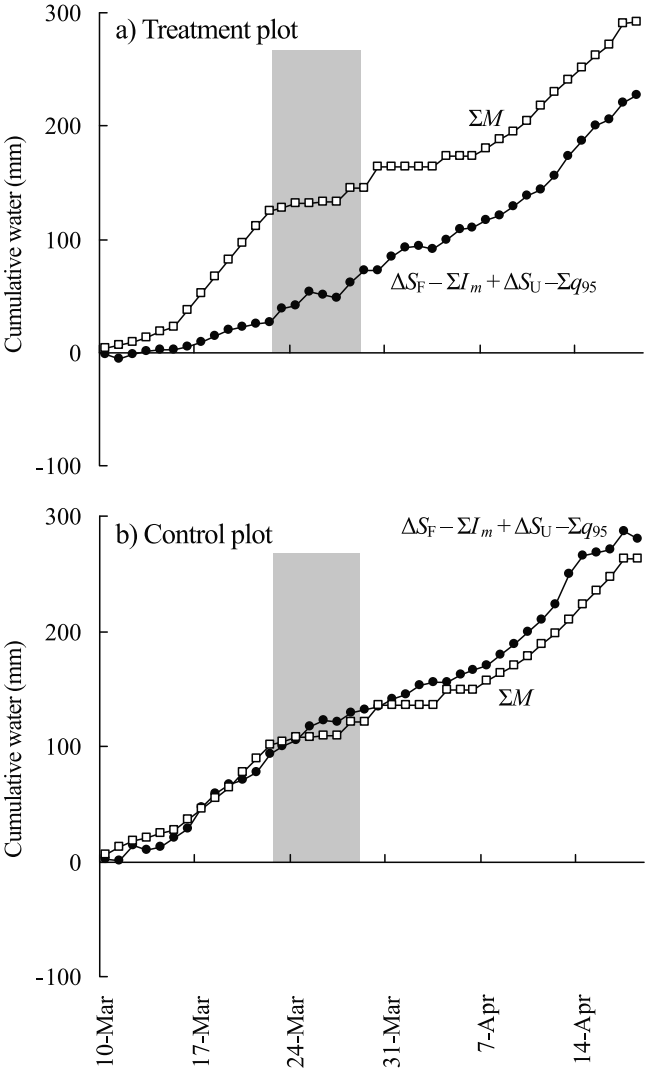

Figure 6. Cumulative values of snowmelt water + precipitation (ΣM) and infiltration ($\Delta S_F - \Sigma I_m + \Delta S_U - \Sigma q_{95}$) in the treatment and control plots during and after the snowmelt period. Snow cover was absent during the shaded period.

[28] Using the soil temperature and heat flux plate data with equation (5), the energy balance calculation showed that the total amount of latent heat (ΔH_l) consumed by the melting of ice in the F layer during the entire soil thawing period starting February 25 was 36.2 MJ m^{-2} in the treatment plot and 12.5 MJ m^{-2} in the control plot (see the auxiliary material for detailed calculation). These are equivalent to total ice melt of 109 mm in the treatment plot and 37 mm in the control plot, and are close to the amount ice on February 25 based on the water balance (see the paragraph above). Therefore, the water balance calculation is consistent with the energetics of soil thawing.

3.3. Snowmelt Infiltration

[29] As described in section 3.1, the frozen layer in the treatment plot persisted during the entire snowmelt period, inhibiting the rapid infiltration of rain and meltwater. To quantify this effect, cumulative snowmelt infiltration was calculated from the beginning of the snowmelt period (March 10) and plotted in Figure 6. The difference between the snowmelt (ΣM) and infiltration ($\Delta S_F - \Sigma I_m + \Delta S_U - \Sigma q_{95}$) curves is the sum of runoff and surface storage (see equation (4)), or the infiltration excess.

[30] Snowmelt rate was small (3.5 mm d^{-1}) during March 10–15, and very little infiltration occurred in the treatment plot (Figure 6a). Snowmelt rate increased to 15 mm d^{-1} during March 16–22, but infiltration rate remained low (3.5 mm d^{-1}) in the treatment plot, indicating that infiltration was impeded by the frozen soil layer. As a result, infiltration excess increased and reached 100 ± 3.5 mm (see the auxiliary material for detailed calculation and uncertainty estimate) on March 22 (Figure 6a), when the snow had melted completely. Surface ponding of meltwater was observed during the snow-free period between March 22 and 28 (shaded area in Figure 6a). The steady increase in cumulative infiltration during this period indicates surface water infiltration. The March 29 snowfall started the second phase of melt. During a relatively cold period from March 29 to April 6, 48 mm of infiltration occurred in the treatment plot, while snowmelt was only 29 mm (Figure 6a), suggesting that the continued infiltration of surface water. During the subsequent warmer period of April 7–17, the infiltration rate (10 mm d^{-1}) was comparable to snowmelt rate (11 mm d^{-1}) in the treatment plot (Figure 6a), indicating relatively unimpeded infiltration through the frozen layer. Based on visual observation, surface ponding ended on April 18. For the entire melt period of March 10–April 18, total snowmelt was 291 mm and total infiltration was 228 ± 62 mm in the treatment plot. Despite the relatively large degree of uncertainty in infiltration estimates, the difference between the amount of snowmelt and infiltration (Figure 6a) clearly indicates that a substantial amount of snowmelt water moved out of the system as surface runoff.

[31] In the control plot, snowmelt and infiltration rates were nearly identical during March 10–22 (Figure 6b), indicating unimpeded infiltration of meltwater. Infiltration rate became larger than snowmelt rate after March 25, when the soil surface was exposed temporarily. This difference continued increasing until April 15 (Figure 6b), suggesting lateral input of runoff water (i.e., negative ΣR in equation (4)) may have occurred from the treatment plot.

[32] Soil water flux was negative (i.e., downward) at all depths in the control plot at the beginning of the snowmelt period (March 1–10) (Figure 7), indicating that the wetting front had already reached the bottom of the soil profile due to the infiltration of rain and snowmelt water on February 26. In contrast, soil water flux below 0.8 m was still upward in the treatment plot during this period (Figure 7), and turned downward during March 11–20, indicating a delayed arrival of the wetting front compared to the control plot. However, the magnitude of downward flux in the treatment plot was much smaller than in the control plot during March 11–20 (Figure 7), indicating that infiltration was impeded by the frozen soil layer. The magnitude of flux was comparable between the two plots during April 1–10 (Figure 7) and thereafter, while the frozen layer was still present in the treatment plot (Figure 3f), indicating that the frozen soil

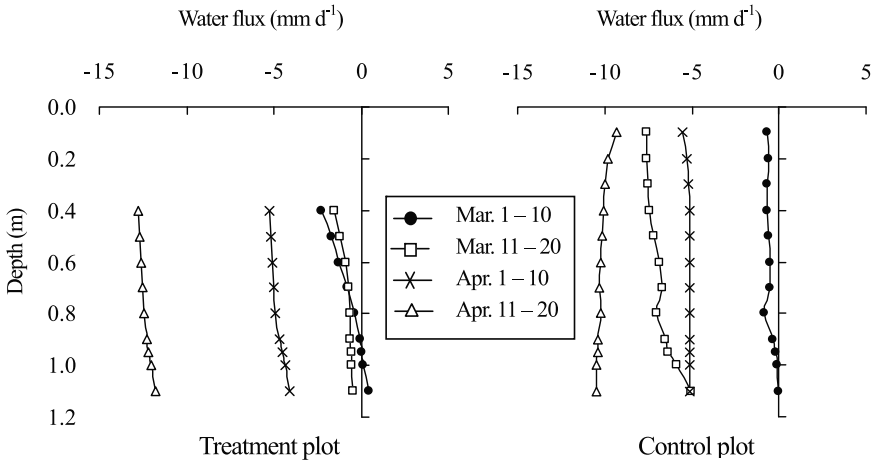

Figure 7. Average soil water flux below the frozen layer over four 10-day periods during soil thawing.

layer did not impede infiltration during these periods, which is consistent with the interpretation of Figure 6a.

4. Discussion

[33] The upward soil water flux at the depth of 0.4 m in the treatment plot was much larger than that in the control plot during the period of snow removal (Figures 3c and 5). In contrast, despite the large magnitude of hydraulic gradient (Figure 3i), the soil water flux at the depth of 0.95 m was small in the treatment plot (Figure 5) (the total flux between December 20 and February 25 was only 3 mm) because unsaturated hydraulic conductivity was very small at low soil matric potential (Figure 4). These results indicate that the influence of upward flow on nutrient transport is restricted to relatively shallow depths, even when frost depth is as deep as 0.4 m. In other regions where soil frost penetrates deeper than 1 m, the upward movement of soil water and nutrients extends to greater depths [*Gray and Granger*, 1986].

[34] During the snowmelt period, most of the meltwater infiltrated in the control plot (Figure 6b), and the infiltration front quickly reached the bottom of the soil profile (Figures 3g and 7). This is consistent with a five-year study conducted by *Iwata et al.* [2008a], who concluded that thin frozen layers did not impede snowmelt infiltration. Therefore, under the present climatic conditions of Tokachi, a large amount of snowmelt water infiltrate to deeper soil horizons and possibly to the water table.

[35] Snowmelt infiltration was clearly impeded in the treatment plot (Figure 6a). To gain insight into the processes that impede infiltration, we note that previous studies elsewhere have shown that infiltration flux is reduced as liquid water refreezes and reduces hydraulic conductivity [*Bayard et al.*, 2005]. In the present study, however, frozen soil temperature in the treatment plot was close to 0°C (−0.11°C of average temperature at the F layer) at the onset of snowmelt on March 10. The energy balance calculation using equation (5) also indicated that the amount of refreezing was undetectable during the period following the rain infiltration event on February 26 or snowmelt after March 10 (see the auxiliary material for detailed calculation). Therefore, the refreezing mechanism cannot account for the reduction in snowmelt infiltration rate. It is more likely that the hydraulic conductivity in the frozen layer was reduced by the preferential blockage of large soil pores by the ice that formed during the pre-melt period, as demonstrated by *Seyfried and Murdock* [1997] using air permeameter. Moreover, previous researches mentioned that horizontal ice lenses can develop near the freezing front, especially in medium textured or silty soils [e.g., *Miller*, 1980], which impede the vertical water movement. Although we did not make direct observation, it is possible that such ice lenses may have contributed to the reduction in infiltration rate.

[36] To corroborate this idea, Figure 8 shows the relative volume of air, ice, and liquid water in the F layer in the treatment plot, expressed as the percentage of total pore volume. Relative ice volume was 43% before the snowmelt and remained nearly constant until March 22, while the snow cover was present (Figure 8). Ice volume rapidly decreased to 26% during March 22–28, while the soil surface was exposed, and remained nearly constant once the soil surface was covered by snow again (Figure 8). The rapid melting of ice was due to the increased heat conduction from the exposed soil surface lacking the snow cover insulation and having low albedo. Since the snowmelt rate was relatively low between March 29 and April 6 (Figure 6), it is impossible to determine whether infiltration in the treatment plot was impeded during this period. However,

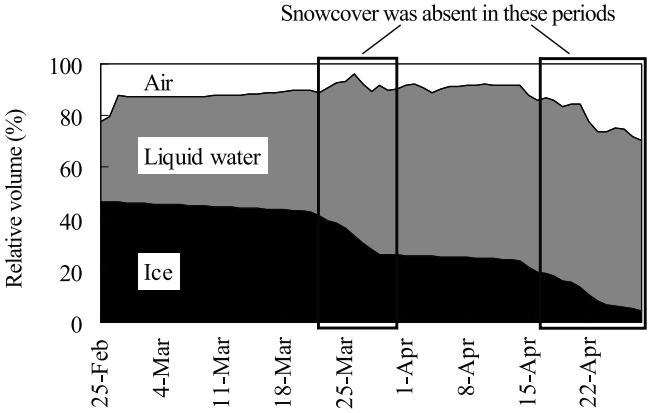

Figure 8. Relative volumes of ice, liquid water, and air in the pore space of F layer in the treatment plot.

infiltration was clearly unimpeded during the high melt-rate period of April 7–17 (Figure 6a), suggesting that a relatively small ice volume during this period was not sufficient to block large soil pores and reduce hydraulic conductivity. Figure 8 shows that total water volume (liquid + ice) in the frozen layer was high prior to the onset of snowmelt. It is well known that high pre-meltwater content reduces snowmelt infiltration in frozen soil [*Kane and Stein*, 1983; *Stähli et al.*, 1996; *Zhao and Gray*, 1999; *Gray et al.*, 2001]. Therefore, a major reduction of snowmelt infiltration in the treatment plot is likely caused partly by the wet conditions of late fall and water supply from the deeper soil layer during the freezing period, which resulted in high pre-melt ice content in the frozen soil layer.

[37] In addition to ice content, soil structure and macropores may also influence infiltration. Macropores may be caused by desiccation cracks, animal burrows, and plant roots, and can transmit large amounts of water through frozen soil layers [*Gray et al.*, 2001; *van der Kamp et al.*, 2003; *Stähli et al.*, 2004]. However, the study site was cultivated during the previous growing season and as such, only small tubular pores (<1 mm) were observed with no large cracks or holes. The absence of macropores may have contributed to the impeded snowmelt infiltration in the treatment plot.

[38] The study plot was flat (<1% slope), which favored the on-site retention of a fairly large amount of surface water. The estimated cumulative infiltration excess in the treatment plot was 100 mm on March 22 and 63 mm on April 18 (Figure 6a). It should be noted that these estimates have a large degree of uncertainty as indicated in section 3.3. Nevertheless, using 63 mm as a rough estimate of the runoff resulting from the 291 mm of snowmelt during March 10–April 17 (Figure 6a), the plot-scale runoff ratio was 0.22 (= 63/291) in the treatment plot, and 0 in the control plot. Therefore, the difference in frost depth could potentially cause a dramatic difference in snowmelt runoff regime. It should be noted, however, that the plot-scale runoff ratio may not directly translate into larger-scale runoff ratio, as some portion of runoff may be retained by larger-scale topographic features such as depressions [*Hayashi et al.*, 2003].

[39] The experiment was designed to evaluate the effect of the timing of snow cover on soil water dynamics and snowmelt infiltration. Other factors including the rates of snowmelt and soil thaw, which may be determined by air temperature, thickness of snow cover, solar radiation, etc., can affect the amount of snowmelt runoff. Further field experiments or numerical simulations will be required to quantify the effects of these other factors.

5. Conclusions

[40] The paired-plot experiment compared the soil water movements during freezing and thawing under the natural condition (control plot), and under a manipulated snow cover (treatment plot). During the 1980s, soil frost penetrated to an average depth of 0.4 m in early winter, while the snow cover on the ground was thin as the development of thick snow cover occurred much later in the 1980s compared to the present. In the treatment plot, we kept removing snow until early January to achieve the maximum frost depth of 0.43 m, similar to the average frost depth during the 1980s. The maximum frost depth in the control plot was 0.11 m. The key findings are: (1) upward soil water flux during the penetration of freezing front was much larger in the treatment plot than in the control plot, (2) snowmelt infiltration was impeded by the frozen soil layer in the treatment plot and unimpeded in the control plot, and (3) a large amount (approximately 100 mm) of infiltration excess occurred during the snowmelt period in the treatment plot, while no infiltration excess occurred in the control plot. Although this experiment did not examine all factors pertinent to soil freezing and snowmelt infiltration, the results clearly indicate a strong influence of the timing of snow cover on soil frost penetration and soil water dynamics.

[41] Based on this experiment and the previous field study by *Iwata et al.* [2008a], the critical frost depth that impedes infiltration and generates runoff in this region is somewhere between 0.2 and 0.4 m. Estimates of the critical frost depth can be further refined by repeated field experiments or numerical experiments using a calibrated model. Such estimates will play an important role in water resources management of the Tokachi region, as they provide the key information regarding the changes in spring runoff and soil infiltration regime. They can also provide tools for agricultural management, such as large-scale snow cover manipulation to mitigate negative impacts associated with the changes [*Hirota*, 2008].

[42] **Acknowledgments.** Unsaturated hydraulic conductivity was measured by Junichi Arima and Kazunobu Kuwao for their M.Sc. thesis work. We thank them for making the data available. We also thank Ken Kawamoto, Satoshi Inoue, Manabu Nemoto, and Yosuke Yanai for helpful suggestions; Greg Langston for editorial comments on an earlier draft; Yuji Tobita, Mitsuru Yamagishi, Koji Tanaka, Noriyuki Goushi, Chikaaki Fujita, Yoshifumi Endo, and Takaaki Endo for their assistance in site instrumentation and laboratory apparatus; and Masamitsu Fujiwara, Hideaki Ogawa, and others in the NARCH Field Operation Section for technical assistance. Miyuki Kikuchi, Shizuka Souma, Emiko Takasugi, and Hisako Tokuji helped with the snow removal operations. The study was partially funded by the Global Environment Research Coordination System Grant and the Global Environment Research Fund (A-0807) from the Japanese Ministry of the Environment and the Invitation Fellowship to MH from the Japan Society for Promotion of Science. Constructive comments by the anonymous reviewers and editors improved the manuscript. The field data presented in this article will be made available under certain conditions regarding the data use by sending a request to Tomoyoshi Hirota (hirota@affrc.go.jp).

References

Bayard, D., M. Stähli, A. Parriaux, and H. Flühler (2005), The influence of seasonally frozen soil on the snowmelt runoff at two Alpine sites in southern Switzerland, *J. Hydrol.*, *309*, 66–84, doi:10.1016/j.jhydrol.2004.11.012.

Cutforth, H., E. G. O'Brien, J. Tuchelt, and R. Rickwood (2004), Long-term changes in the frost-free season on the Canadian prairies, *Can. J. Plant Sci.*, *84*, 1085–1091.

Decker, K. L. M., D. Wang, C. Waite, and T. Scherbatskoy (2003), Snow removal and ambient air temperature effects on forest soil temperatures in northern Vermont, *Soil Sci. Soc. Am. J.*, *67*, 1234–1242.

Doering, E. J. (1965), Soil-water diffusivity by the one-step method, *Soil Sci.*, *99*, 322–326, doi:10.1097/00010694-196505000-00005.

Flerchinger, G. N., M. S. Seyfried, and S. P. Hardegree (2006), Using soil freezing characteristics to model multi-season soil water dynamics, *Vadose Zone J.*, *5*, 1143–1153.

Frauenfeld, O. W., T. Zhang, and R. G. Barry (2004), Interdecadal changes in seasonal freeze and thaw depths in Russia, *J. Geophys. Res.*, *109*, D05101, doi:10.1029/2003JD004245.

Gray, D. M., and R. J. Granger (1986), In situ measurement of moisture and salt movement in frozen soils, *Can. J. Earth Sci.*, *23*, 696–704.

Gray, D. M., B. Toth, L. Zhao, J. W. Pomeroy, and R. J. Granger (2001), Estimating areal snowmelt infiltration into frozen soils, *Hydrol. Processes*, *15*, 3095–3111, doi:10.1002/hyp.320.

Hardy, J. P., P. M. Groffman, R. D. Fitzhugh, K. S. Henry, A. T. Welman, J. D. Demers, T. J. Fahey, C. T. Driscoll, G. L. Tierney, and S. Nolan (2001), Snow depth manipulation and its influence on soil frost and water dynamics in a northern hardwood forest, *Biogeochemistry*, *56*, 151–174, doi:10.1023/A:1013036803050.

Hasegawa, S., and T. Sakayori (2000), Monitoring of matrix flow and bypass flow through the subsoil in a volcanic ash soil, *Soil Sci. Plant Nutr.*, *46*, 661–671.

Hayashi, M., G. van der Kamp, and R. Schmidt (2003), Focused infiltration of snowmelt water in partially frozen soil under small depressions, *J. Hydrol.*, *270*, 214–229, doi:10.1016/S0022-1694(02)00287-1.

Hayashi, M., T. Hirota, Y. Iwata, and I. Takayabu (2005), Snowmelt energy balance and its relation to foehn events in Tokachi, Japan, *J. Meteorol. Soc. Jpn.*, *83*, 783–798, doi:10.2151/jmsj.83.783.

Hirota, T. (2008), Decreasing soil-frost depth in eastern Hokkaido and its impact on agriculture (in Japanese), *Tenki*, *55*, 548–551.

Hirota, T., M. Fukumoto, and T. Watanabe (2001), Soil heat flux, water heat storage and forest heat storage (in Japanese), in *Method of Surface Flux Measurements*, *Meteorol. Res. Note 199*, edited by O. Tsukamo and N. Monji, pp. 141–151, Meteorol. Soc. Jpn., Tokyo.

Hirota, T., Y. Iwata, M. Hayashi, S. Suzuki, T. Hamasaki, R. Sameshima, and I. Takayabu (2006), Decreasing soil-frost depth and its relation to climate change in Tokachi, Hokkaido, Japan, *J. Meteorol. Soc. Jpn.*, *84*, 821–833, doi:10.2151/jmsj.84.821.

Hohmann, M. (1997), Soil freezing—The concept of soil water potential. State of the art, *Cold Reg. Sci. Technol.*, *25*, 101–110, doi:10.1016/S0165-232X(96)00019-5.

Iwata, Y., and T. Hirota (2005a), Development of tensiometer for monitoring soil-water dynamics in a freezing and snow covered environment, *J. Agric. Meteorol.*, *60*, 1065–1068.

Iwata, Y., and T. Hirota (2005b), Monitoring over-winter soil water dynamics in a freezing and snow covered environment using thermally insulated tensiometer, *Hydrol. Processes*, *19*, 3013–3019, doi:10.1002/hyp.5813.

Iwata, Y., M. Hayashi, and T. Hirota (2008a), Comparison of snowmelt infiltration under different soil-freezing conditions influenced by snow cover, *Vadose Zone J.*, *7*, 79–86, doi:10.2136/vzj2007.0089.

Iwata, Y., M. Hayashi, and T. Hirota (2008b), Effects of snow cover on soil heat flux and freeze-thaw processes, *J. Agric. Meteorol.*, *64*, 301–309, doi:10.2480/agrmet.64.4.12.

Johansen, O. (1977), Experimental investigation of thermal conductivity in soil materials, in *Thermal Conductivity of Soils*, edited by O. Johansen, pp. 177–223, Cold Reg. Res. Eng. Lab., Hanover, N. H.

Johnsson, H., and L.-C. Lundin (1991), Surface runoff and soil water percolation as affected by snow and soil frost, *J. Hydrol.*, *122*, 141–159, doi:10.1016/0022-1694(91)90177-J.

Kane, D. L., and J. Stein (1983), Water movement into seasonally frozen soil, *Water Resour. Res.*, *19*, 1547–1557, doi:10.1029/WR019i006p01547.

Kasubuchi, T. (1975), The effect of soil moisture on thermal properties in some typical Japanese upland soils, *Soil Sci. Plant Nutr.*, *21*, 107–112.

Luetschg, M., M. Lehning, and W. Haeberli (2008), A sensitivity study of factors influencing warm/thin permafrost in the Swiss Alps, *J. Glaciol.*, *54*, 696–704, doi:10.3189/002214308786570881.

Miller, R. D. (1980), Freezing phenomena in soils, in *Applications of Soil Physics*, edited by D. Hillel, pp. 254–299, Academic, San Diego, Calif.

Nyberg, L., M. Stähli, P.-E. Mellander, and K. H. Bishop (2001), Soil frost effects on soil water and runoff dynamics along a boreal forest transect: 1. Field investigations, *Hydrol. Processes*, *15*, 909–926, doi:10.1002/hyp.256.

Oka, T. (2000), *Geological features and its explanation at Middle Tokachi Plain* (in Japanese), Geol. Surv. of Hokkaido, Sapporo, Japan.

Øygarden, L. (2003), Rill and gully development during an extreme winter runoff event in Norway, *Catena*, *50*, 217–242, doi:10.1016/S0341-8162(02)00138-8.

Sauer, T. J. (2002), Heat flux density, in *Methods of Soil Analysis, Part 4. Physical Methods*, edited by J. H. Dane and G. C. Topp, *Soil Sci. Soc. Am. Book Ser.*, *5*, 1233–1248.

Seyfried, M. S., and M. D. Murdock (1997), Use of air permeability to estimate infiltrability of frozen soil, *J. Hydrol.*, *202*, 95–107, doi:10.1016/S0022-1694(97)00061-9.

Shanley, J. B., and A. Chalmers (1999), The effect of frozen soil on snowmelt runoff at Sleepers River, Vermont, *Hydrol. Processes*, *13*, 1843–1857, doi:10.1002/(SICI)1099-1085(199909)13:12/13<1843::AID-HYP879>3.0.CO;2-G.

Stähli, M. (2005), Freezing and thawing phenomena in soils, in *Encyclopedia of Hydrological Sciences,* vol. 2, edited by M. G. Anderson, pp. 1069–1076, John Wiley, New York.

Stähli, M., P.-E. Jansson, and L.-C. Lundin (1996), Preferential water flow in a frozen soil–a two-domain model approach, *Hydrol. Processes*, *10*, 1305–1316, doi:10.1002/(SICI)1099-1085(199610)10:10<1305::AID-HYP462>3.0.CO;2-F.

Stähli, M., P.-E. Jansson, and L.-C. Lundin (1999), Soil moisture redistribution and infiltration in frozen sandy soils, *Water Resour. Res.*, *35*, 95–103, doi:10.1029/1998WR900045.

Stähli, M., D. Bayard, H. Wydler, and H. Flühler (2004), Snowmelt infiltration into Alpine soils visualized by dye tracer technique, *Arct. Antarct. Alp. Res.*, *36*, 128–135, doi:10.1657/1523-0430(2004)036[0128:SIIASV]2.0.CO;2.

Stein, J., and D. L. Kane (1983), Monitoring the unfrozen water content of soil and snow using time domain reflectometry, *Water Resour. Res.*, *19*, 1573–1584, doi:10.1029/WR019i006p01573.

Suzuki, S. (2004), Dependence of unfrozen water content in unsaturated frozen clay soil on initial soil moisture content, *Soil Sci. Plant Nutr.*, *50*, 603–606.

Thorud, D. B., and D. P. Duncan (1972), Effects of snow removal, litter removal and soil compaction on soil freezing and thawing in a Minnesota Oak Stand, *Soil Sci. Soc. Am. Proc.*, *36*, 153–157.

Unoki, K., T. Yamamoto, T. Inoue, T. Nagasawa, and H. Okazawa (2003), River water quality and hydrological condition of dairy farming watershed during snowmelt and ground thawing period (in Japanese with English abstract), *Trans. Jpn. Soc. Irrig. Drain. Reclam. Eng.*, *228*, 9–15.

van der Kamp, G., M. Hayashi, and D. Gallén (2003), Comparing the hydrology of grassed and cultivated catchments in the semi-arid Canadian prairies, *Hydrol. Processes*, *17*, 559–575, doi:10.1002/hyp.1157.

Yamazaki, Y., F. Tsuchiya, and O. Tsuji (2003), Measurement and estimation of thermal conductivity of quartz-containing frozen and unfrozen soils (in Japanese with English abstract), *Trans. Jpn. Soc. Irrig. Drain. Reclam. Eng.*, *226*, 43–51.

Zhao, L., and D. M. Gray (1999), Estimating snowmelt infiltration into frozen soils, *Hydrol. Processes*, *13*, 1827–1842, doi:10.1002/(SICI)1099-1085(199909)13:12/13<1827::AID-HYP896>3.0.CO;2-D.

S. Hasegawa, Field Science Center for Northern Biosphere, Hokkaido University, Kita11 Nishi 10, Kita-ku, Sapporo, Hokkaido, 060-0811, Japan. (hasegawa@env.agr.hokudai.ac.jp)

M. Hayashi, Department of Geoscience, University of Calgary, 2500 University Dr. NW, Calgary, AB T2N 1N4, Canada. (hayashi@ucalgary.ca)

T. Hirota, National Agricultural Research Center for Hokkaido Region, Hitsujigaoka Toyohira-ku Sapporo, Hokkaido 062-8555, Japan. (hirota@affrc.go.jp)

Y. Iwata, National Agricultural Research Center for Hokkaido Region, NARO, Shinsei, Memuro, Hokkaido, 082-0081, Japan. (hirota@affrc.go.jp; iwatayuk@affrc.go.jp)

S. Suzuki, Department of Bioproduction and Environment Engineering, Tokyo University of Agriculture, 1-1-1 Sakuragaoka, Setagaya, Tokyo, 156-8502, Japan. (s4suzuki@nodai.ac.jp)